Tribology International 123 (2018) 209–215

Contents lists available at ScienceDirect

Tribology International

journal homepage: www.elsevier.com/locate/triboint

On the load dependence of friction: Role of the long-range elastic coupling

O.M. Braun [a,b], N. Miyashita [c], H. Fujii [c], B.N.J. Persson [b,*,1]

[a] Institute of Physics, National Academy of Sciences of Ukraine, 03028 Kiev, Ukraine
[b] PGI, FZ-Jülich, 52425 Jülich, Germany
[c] The Yokohama Rubber Company, 2-1 Oiwake, Hiratsuka, Kanagawa 254-8601, Japan

ARTICLE INFO

Keywords:
Elastic coupling
Stick-slip
Friction coefficient
Earthquake model

ABSTRACT

When an elastic block is squeezed in contact with a substrate the contact will in general consist of many asperity contact regions. During sliding the long-range elastic coupling between the contact regions have a big influence on the sliding dynamics: when the loading force increases the density of contact regions increases, which affects the lateral coupling between the contact region, and introduces a dependence of the friction force on the loading force. Here we present a full three-dimensional model study of the role of the elastic coupling on the friction force. The theory is applied to rubber friction, but the mechanism for the dependence of the friction coefficient on the load is relevant for non-rubber materials as well.

1. Introduction

The Amontons friction law states that the friction force $F_f = \mu F_N$ is proportional to the normal force or load F_N, and is found to hold remarkable well in many practical applications [1–3]. For elastic solids with nominally flat but randomly rough surfaces, contact mechanics theories and numerical simulations show that the contact area A is proportional to the nominal contact pressure $p_0 = F_N/A_0$, where A_0 is the nominal contact area [4–12]. If it is assumed that a characteristic frictional shear stress τ_f acts in the area of real contact, then the friction coefficient $\mu = \tau_f A/(p_0 A_0)$ will be independent of the pressure p_0, i.e., independent of the normal load $F_N = p_0 A_0$. There are many reasons why the Amontons friction law may fail, and in this work we discuss a fundamental and very general mechanism, which is also very important for rubber friction, e.g., for the friction between tires and road surfaces [13,14].

The explanation of the Amontons friction law for a rough interface, first proposed by Bowden and Tabor, is based on a static picture. However, the situation may change drastically for a moving interface. Kinetics of the multi-contact interface is typically described with the help of an earthquakelike model [15,16], where the contact of two surfaces is due to many microcontacts which break and restore during relative motion of the surfaces (e.g., see Ref. [17] and references therein). At small driving velocities, F_k increases linearly with speed, $F_k(v) \approx \eta v$. Indeed, if the slider moves slow enough, thermal fluctuations sooner or later will break all contacts. The more slowly the slider moves, the longer time all contacts are given to receive a fluctuation above their respective threshold, therefore the smaller the resulting friction force is. This linear $F_k \approx \eta v$ dependence could be represented as a (characteristically large) effective viscosity η of an ultra-thin lubricant layer [18,19].

At high driving velocities the kinetic friction force exhibits the opposite behavior, it decreases when v grows, roughly as $F_k(v) \sim f_s v^*/v$, due to aging effects. Indeed, after snapping, the contact slips for some time, then it is reformed again and grows in size. The faster the slider moves, the shorter time the contacts are left to be reformed and grow. Thus, the kinetic friction force $F_k(v)$ increases with v at low v up to a maximum at $v_m \sim (f_s v^*/\eta)^{1/2}$ and then decreases. On the decreasing branch of $F_k(v)$, i.e. for $v > v_m$, the slider motion may become unstable and change from smooth sliding to stick-slip motion: if the slider velocity increases due to a fluctuation, the friction force decreases, and the slider accelerates.

Solid objects usually have surface roughness on many length scales. For the contact between elastic solids, the longest surface roughness results in macro-asperity contact regions. As the interface is observed at increasing magnification one observes that the macroasperity contact regions actually consist of many microcontacts and thus should exhibit the $F_k(v)$ dependence described above. Due to variation in asperity sizes, surface contamination and other surface properties, different macrocontacts will be characterized by $F_k(v)$ dependences with different v_m values. For a nonrigid slider, its elasticity produces an interaction be-

* Corresponding author.
E-mail address: b.persson@fz-juelich.de (B.N.J. Persson).
[1] www.MultiscaleConsulting.com.

https://doi.org/10.1016/j.triboint.2018.01.018
Received 15 September 2017; Received in revised form 5 January 2018; Accepted 8 January 2018
Available online 12 January 2018

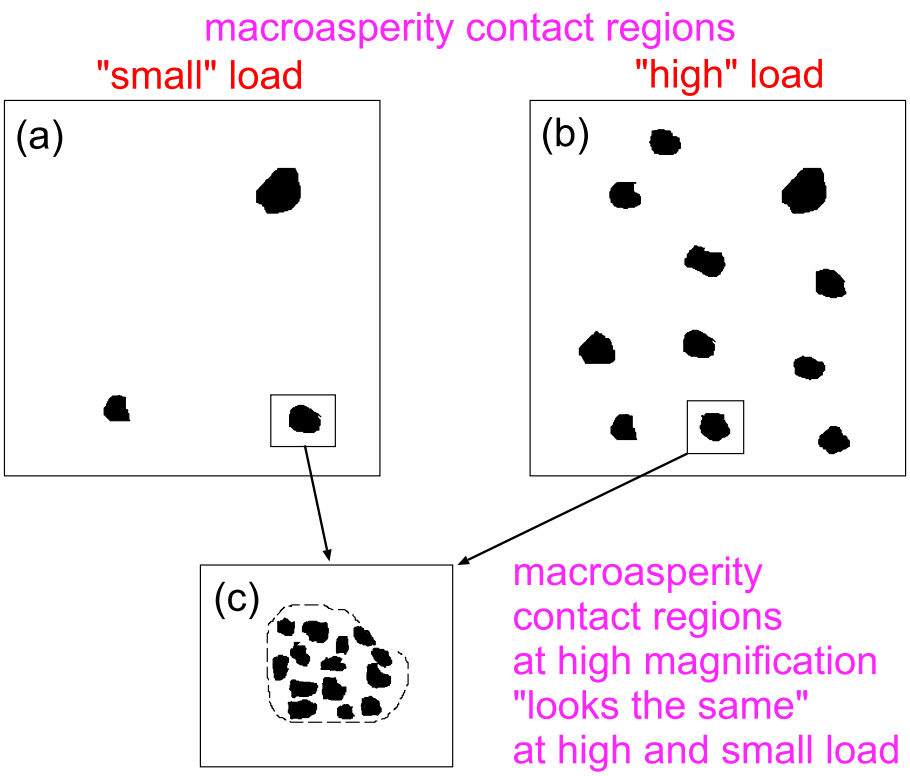

Fig. 1. The contact region between two solids with random surface roughness. In (a) and (b) the black regions denote the macroasperity contact regions, which are the contact spots observed at low magnification where only the most long-wavelength roughness can be detected. When the normal force (load) increases, the number of macroasperity contact regions increases proportional to the load, but (for an infinite system) the normalized probability distribution of macroasperity contact sizes is unchanged. When we increase the magnification the macroasperity contact regions are observed to consist of smaller microasperity contact regions. However, the nature of the internal structure of the macroasperity contact regions, e.g., the distribution of sized of the microasperity contact region, does not depend on the normal load.

tween the macrocontacts: as soon as a contact fails, the forces on nearby contacts must increase [20] and may provoke their breaking and sliding as well.

In the following we consider surfaces which are nominally flat but exhibit roughness at length scales much shorter than the linear size L of the surface. Such surfaces have surface roughness power spectra with a roll-off region for small wavenumbers [21]. When such surfaces are observed at low magnification one observes only the most long wavelength part of the surface roughness, and the contact appears to consist of randomly distributed macro-asperity contact regions [5]. When a macroasperity contact region is observed at higher magnification, shorter wavelength roughness is observed and the macroasperity contact region breaks up into smaller microasperity contact regions.

Contact mechanics studies show that for large systems with increasing pressure p_0, existing contact areas grow and new contact areas form in such a way that the (normalized) interfacial stress distribution, and also the size distribution of contact spots, are independent of the squeezing pressure (see Fig. 1) [4–7]. When this is the case the macroscopic friction force will be proportional to the normal force even when the friction force acting on the asperity contact regions at the smallest length scale depends non-linearly on the asperity contact area. In this case, since the distribution of microasperity contact regions within the macroasperity contact regions does not depend on the load (see Fig. 1), the only thing which could influence the sliding friction is the concentration (a real density) of macro-asperity contact regions, which increases proportional to p_0.

In this work we present a full three-dimensional (3D) model for the elastic coupling between the macroasperity contact regions. This is a generalization of the 2D-model studied in Refs. [16,22]. We show that the lateral coupling between the contact regions influences the stick-slip dynamics of the contact regions and results in a dependence of the friction coefficient on the load, similarly to what was observed in recent rubber friction experiments [23,24], and also in the present paper where new experimental data are presented for a tire tread rubber sliding on a concrete surface.

This paper is organized as follows: In Sec. 2 we present a qualitative discussion about why (or how) the contact pressure may influence the friction coefficient. In Sec. 3 we present new experimental results for the dependence of the friction coefficient on the nominal contact pressure. Section 4 describes a simple 3D-model used for calculating the dependence of the friction force on the normal load, and Sec. 5 present numerical results and discussion. Section 6 presents the summary and conclusion.

2. Qualitative discussion

For velocities $v \ll v_m$ the rubber in (almost) all macro-asperity contact regions slips relative to the substrate with the same velocity v as the upper surface of the rubber block. In that case the elastic (or rather viscoelastic) coupling between the rubber macroasperity contact regions is not changing in time, and it is basically irrelevant for the friction. However, for velocities $v > v_m$ the rubber friction decreases with increasing sliding speed. Now, if the driving force is constant, this results in an unstable branch of the $\mu(v)$-curve, where the rubber block accelerates. If instead the upper surface of the block would be rigidly driven with a constant velocity $v > v_m$, the bottom surface of the block would perform stick-slip motion.

With the same arguments, one expects that the rubber in the macroasperity contact regions will perform stick-slip motion for $v > v_m$. However, due to stochastic fluctuations in the nature of the macroasperity contact regions (e.g., due to local fluctuations in the roughness or surface contamination) one expects not a sharp onset velocity for stick-slip motion at the macroasperity level, but a distribution of onset velocities. Therefore, we expect that close to the friction maximum, but for $v < v_m$, some contact regions will perform stick-slip motion. In this case the motion of a macroasperity contact region depends on the motion of other macroasperity contact regions. Thus, we expect some correlation in the local stick-slip events when the velocity is close to the point where the friction coefficient is maximal. For example, if the rubber in a macroasperity contact region slips into a state where the shear force acting on it

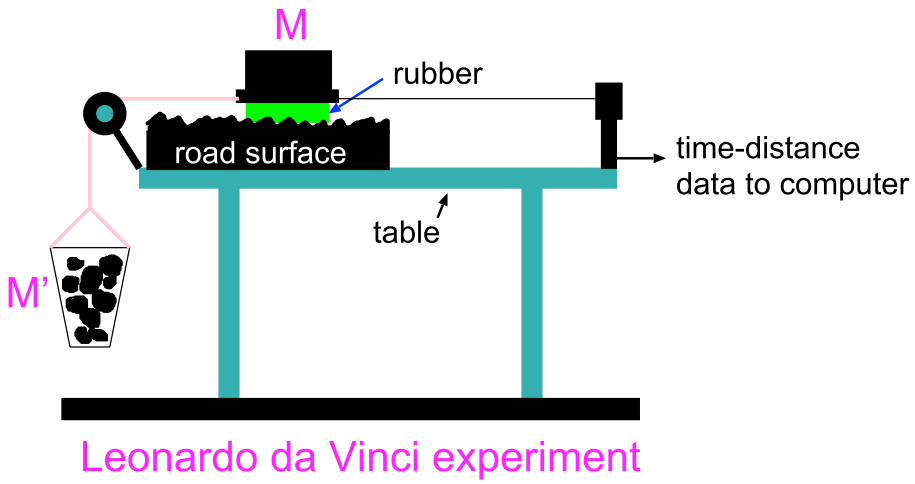

Fig. 2. Simple friction tester (schematic) used for obtaining the friction coefficient $\mu = M'/M$ as a function of the sliding speed. The sliding distance is measured using a distance sensor and the sliding velocity obtained by dividing the sliding distance with the sliding time.

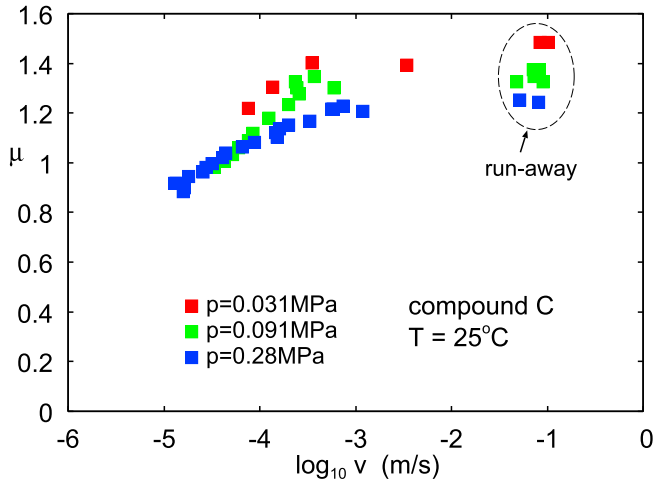

Fig. 3. The kinetic friction coefficient as a function of the logarithm of the sliding speed for rubber tread compound C for the nominal contact pressures $p_0 = 0.031$ (red squares), 0.091 (green squares) and 0.28 MPa (blue squares), and the temperature $T \approx 25°C$. The experimental data within the dashed ellipse correspond to unsteady (accelerated) motion. (For interpretation of the references to colour in this figure legend, the reader is referred to the Web version of this article.)

vanishes, the tangential force lost in this contact region will distribute itself on the other macroasperity contact regions, where the shear stress now may increase to the point of resulting in local slip, and so on. Clearly, this lateral coupling, and the way the stress redistributes itself in response to a local slip at a macroasperity contact region, will depend on the average separation between the macroasperity contact regions, and hence on the concentration of the macroasperity contact regions, which increases with increasing nominal contact pressure.

Here we present a full 3D-model to study in greater detail the mechanism discussed above, and we show that the lateral coupling between the macro-asperity contact regions gives rise to a friction coefficient μ which depends on the load for v close to v_m.

3. Leonardo da Vinci experiment

The measured data was obtained using the set-up shown in Fig. 2. The slider consists of two rubber blocks glued to a wood plate. One block is at the front of the wood plate and the other at the end of the wood plate, and the nominal contact area $A_0 = 10\,\text{cm}^2$. The normal force is generated by adding lead blocks (total mass M) on top of the wood plate. Similarly the driving force is generated by adding lead blocks in the container M' in Fig. 2. In the Leonardo da Vinci experiments the rubber blocks are run in on the substrates on which the measurements are done.

The sliding distance as a function of time is measured using a distance sensor. This simple friction tester can be used for obtaining the friction coefficient $\mu = M'/M$ as a function of sliding velocity and nominal contact pressure $p_0 = Mg/A_0$. Note that with this set-up the driving force is specified, and the velocity dependence of the steady-state friction can be studied only on the branch of the $\mu(v)$ curve where the friction coefficient increases with increasing speed. In the experiments the motion is either steady sliding (with small fluctuations in the sliding speed from surface inhomogeneities), or the block accelerates (but no periodic stick-slip motion can occur in this set-up). This differs from the theoretical model used in Secs. 4 and 5, where the velocity of the upper surface of the rubber block is specified, and where in principle the bottom surface of the rubber block could perform periodic stick-slip oscillations. Nevertheless, if steady sliding occurs, it does not matter if the driving force or driving velocity is specified.

All experiments was performed on a tire tread rubber compound. As substrate we used a concrete surface. Fig. 3 shows the friction coefficient as a function of the logarithm of the sliding speed. Results are shown for the nominal contact pressures $p_0 = 0.031$ (red squares), 0.091 (green squares) and 0.28 MPa (blue squares), and the temperature $T \approx 25°C$. Note that as the contact pressure increases the friction coefficient decreases in a velocity range close to the local maximum ($v_m \approx 10^{-3}$ m/s).

Before each experiment both the concrete surface and the rubber block surfaces were cleaned with a soft brush to remove contamination (wear particles). Fig. 4(a) and (b) show optical pictures of the rubber blocks after the sliding experiment with the load $F_N \approx 300$ N at the highest sliding speed. Note that rubber wear particles, in the form of cylinder-shaped rolls, can be observed on the front (in the sliding direction) rubber block as demonstrated in Fig. 4(a).

To test the influence of the wear particles on the friction results presented in Fig. 3 we performed one experiment (for $p_0 = 0.28$ MPa) where we first increased the velocity from lowest velocity up to the highest velocity (where the wear rate probably is highest), and then reduced the sliding speed down to a similar value as in the first measurement. The rubber blocks were cleaned only before the start of the first measurement, so we expect rubber wear particles to accumulate on the rubber blocks during the test. Fig. 5 shows the results. The full squares correspond to measured data when increasing the driving force (corresponding to increasing sliding speed), while the open squares correspond to decreasing driving force. Note that there is only a very

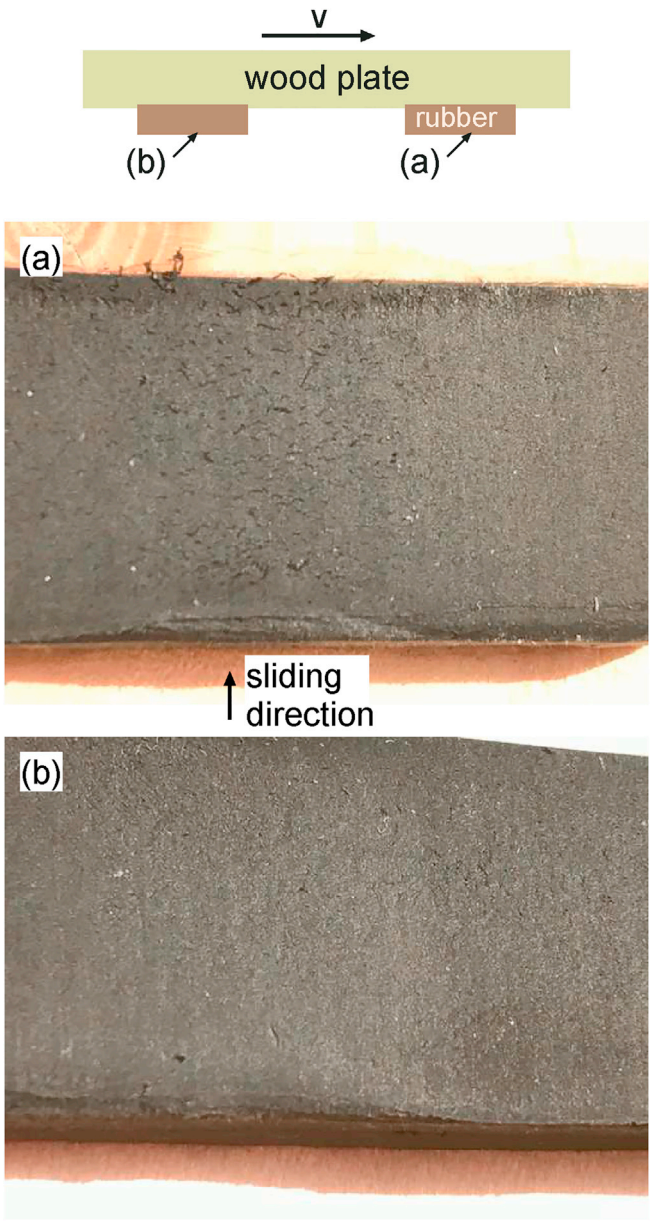

Fig. 4. Optical pictures of the rubber blocks after the sliding experiment with the load $F_N \approx 300$ N at the highest sliding speed. (a) Refer to the rubber block located at the front (in the sliding direction) and (b) at the back of the wood plate. Note that in picture (a) rubber wear particles in the form of cylinder-shaped rolls can be observed.

small reduction in the friction coefficient during the cycle where the sliding speed is reduced as compared to the cycle when it is increased. Hence we conclude that trapped wear particles have only a small influence on the observed friction.

4. Block-and-spring model

Our model is similar to the Burridge and Knopoff spring-block model [15] used to study some aspects of earthquake dynamics and boundary lubrication [16,17]. In this model the top block (the slider) is coupled with the bottom block (the substrate), assumed to be rigid and fixed, by a set of frictional contacts, see Fig. 6.

The slider has the shape of parallelepiped of size $N_x a \times N_y a \times N_z a$; its motion is described by the elastic equation [20,25] (we assume isotropic slider)

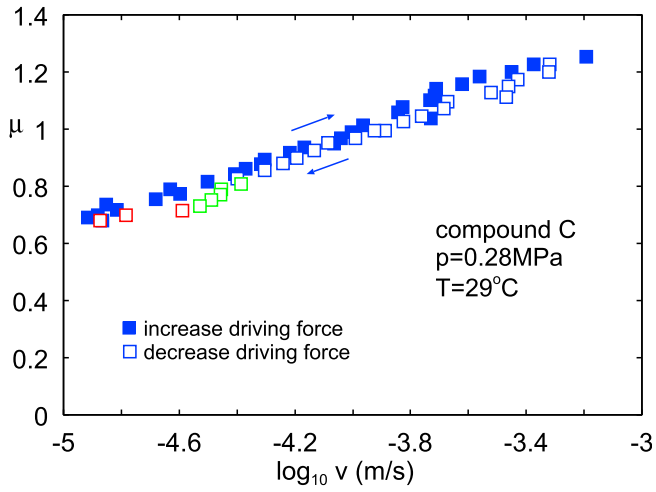

Fig. 5. The kinetic friction coefficient as a function of the logarithm of the sliding speed for rubber tread compound C for the nominal contact pressure $p_0 = 0.28$ MPa and the temperature $T \approx 29$°C (blue symbols). The green and red open squares were obtained for the temperatures $T \approx 26$°C and $T \approx 24$°C, respectively. The full squares correspond to measured data when increasing the driving force (corresponding to increasing sliding speed), while the open squares correspond to decreasing driving force. The rubber blocks were cleaned before the first measurement only. (For interpretation of the references to colour in this figure legend, the reader is referred to the Web version of this article.)

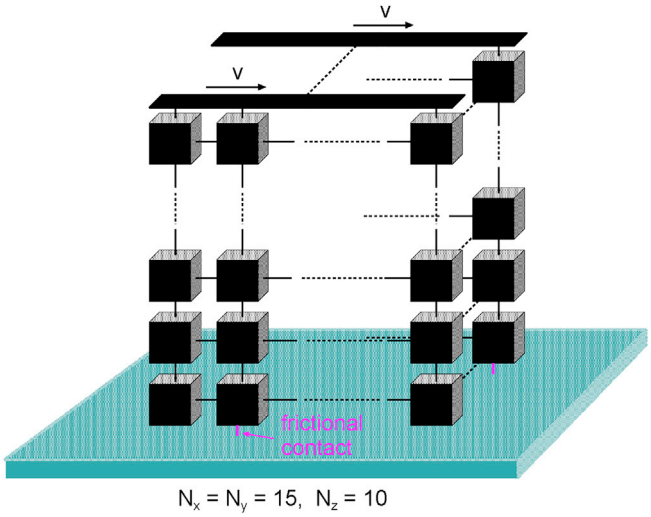

Fig. 6. The friction model studied in this paper. The sliding block (mass M) is discretized into $N = N_x N_y N_z$ mass points (mass $m = M/N$), in the figure indicated as small blocks, which are connected by viscoelastic springs (black lines). A fraction θ of the mass points at the bottom surface of the sliding block are connected by frictional coupling to the substrate (pink lines). The upper surface of the sliding block is connected to a rigid surface with viscoelastic springs. The rigid surface moves with the velocity v parallel to the substrate. The parameter θ is proportional to the normal load (see text for more details). (For interpretation of the references to colour in this figure legend, the reader is referred to the Web version of this article.)

$$\frac{\partial^2 \mathbf{u}}{\partial t^2} = G_1 \nabla^2 \mathbf{u} + G_2 \nabla(\nabla \cdot \mathbf{u}), \tag{1}$$

where $\mathbf{u}(\mathbf{R})$ is the 3D displacement vector in the slider, $\mathbf{R} = (x,y,z)$, $G_1 = E/[2(1+\nu)\rho] = c_t^2$ and $G_2 = (1+2\nu)G_1 = c_l^2 - c_t^2$, E, ν and ρ are the Young modulus, Poisson ratio and mass density of the slider correspondingly, and c_l (c_t) is the longitudinal (transverse) sound speed.

For numerical solution of Eq. (1) we discretized it [26], so that the

slider consists of $N = N_x N_y N_z$ rigid a^3-cubes which interact elastically according to Eq. (1). In the x and y directions we use periodic boundary conditions. The top surface of the slider is pressed in the z direction by the normal force (load)

$$F_N = \varepsilon\theta P_0 N_x N_y a^2, \tag{2}$$

where P_0 is the maximal nominal contact pressure (the parameters θ and ε will be discussed below).

The top surface of the slider is driven through $N_x N_y$ transverse springs of elastic constant $k = Ea/[2(1+\nu)]$ in the x direction with a velocity v. The sum of forces in these springs is the friction force F_f. The friction coefficient is then defined as $\mu = \langle F_f\rangle/F_N$, where $\langle\ldots\rangle$ is the time average in the steady state regime.

The bottom surface of the slider is coupled by frictional contacts with the base; these contacts describe the macroasperity contact regions. Namely, the slider is coupled with the substrate by $N_c = \theta N_x N_y$ frictional contacts with a *random spatial distribution*. For a contact of rough surfaces the dimensionless parameter $\theta \le 1$ is directly proportional to the load. The force acting on the i'th block to which the contact is attached, depends on the block velocity v_i: it increases at small v, reaches a maximum around some v_m and then decreases. To be specific, we use the dependence found experimentally [24]:

$$f(v_i, v_i^*) = \varepsilon f_0 \exp(-c\xi_i)\mathrm{sign}(v_i) + m\eta_c v_i\,, \tag{3}$$

$$\xi_i = \left[\log_{10}\left(|v_i|/v_i^*\right)\right]^2, \tag{4}$$

where $f_0 = a^2\tau_f$, τ_f is the shear stress at the macroasperity, c is a numerical constant, $m = \rho a^3$ is the mass of the a^3-cube, η_c is the viscous damping due to motion of the macroasperity over the substrate, and the parameters v_i^* are randomly distributed around some value v_m.

In simulation we used $N_x = N_y = 15$ (or $N_x = N_y = 30$ for Fig. 9) and $N_z = 10$ so that the slider consists of $N = 2250$ (or $N = 9000$) blocks (a^3-cubes), each of linear size $a = 0.1$ mm and mass $m = 10^{-9}$ kg, and the interface consists of maximum $N_x N_y = 225$ (or 900) contacts. The elastic block (which we denote as "rubber") has the mass density $\rho = 10^3$ kg/m^3, the Young modulus $E = 10$ MPa and the Poisson ratio $\nu = 0.5$. The maximal nominal pressure is $P_0 = 10^6$ Pa.

Because we drive the slider by the external force, the energy is continuously pumped into the system and has to be removed to avoid infinite increasing of the slider temperature. For this purpose, between the nearest neighboring blocks i and j we added the viscous damping force $f_{ij} = -m\eta(v_i - v_j)$ with the damping coefficient $\eta = 0.1\omega_0$, where $\omega_0 = c_l/a = 10^6$ s^{-1} is the characteristic frequency of the slider, so that the system dynamics is underdamped. Another channel of dissipation is the viscous damping η_c in Eq. (3) because of motion of the macroasperity over the substrate; we took $\eta_c = 0.1\omega_0$ as well.

The frictional interface is parameterized as follows [24]: $\tau_f = 6.5 \times 10^6$ Pa, $c = 0.1$, and the parameters v_i^* are randomly distributed around the value $v_m = 1$ mm/s (in detail, the values $\log_{10} v_i^*$ are uniformly distributed within the interval $[\log_{10} v_m - \delta, \log_{10} v_m + \delta]$ with $\delta = 0.5$).

The "scaling" parameter ε in Eqs. (2) and (3) was introduced because of the following technical problem [19,26]. The characteristic time scale of the slider is $\tau_0 = 2\pi/\omega_0 \approx 6.28 \times 10^{-6}$ s, while the characteristic time scale of the frictional contacts is $\tau_c = v_0 m/f_0 \approx 1.54 \times 10^{-11}$ s which is more than five orders of magnitude smaller. Using the value $\varepsilon = 10^{-2}$, we were able to simulate the system within a reasonable computer time (of course, we checked that changing of ε does not modify our results, at least qualitatively).

During simulation we saved the total driving force $f(t) = (N_x N_y)^{-1}\sum_{i=1}^{N_x N_y} k[vt - x_i(t)]$, where $x_i(t)$ is the coordinate of the ith block at the top surface of the slider, and then calculated the friction coefficient for the steady sliding.

5. Simulation results and discussion

The simulation results are presented in Figs. 7 and 8. Fig. 7 shows that for the lower driving velocity $v = 3 \times 10^{-4}$ m/s the friction is almost independent of load, while for $v = v_m = 10^{-3}$ m/s the friction may decrease by more than 15% when the load grows, in a good agreement with the experiment.

Analyzing the simulation results in more detail, we found the following explanation of this effect. Let v be the velocity of the drive. A single (isolated) contact i moves with a constant velocity v if $v < v_i^*$, and hence experiences the constant friction force $f(v, v_i^*)$. However, if $v > v_i^*$, its motion may become unstable, and the contact will undergo stick-slip motion. In the latter case, the contact accelerates during slip, and the force drops, so the averaged force from this contact is lower than $f(v, v_i^*)$; the effect is the larger, the lower is the damping parameter η_c. For a set of non-interacting contacts, the driving force in the steady state is approximately equal to the sum of the forces from all contacts, and thus slightly

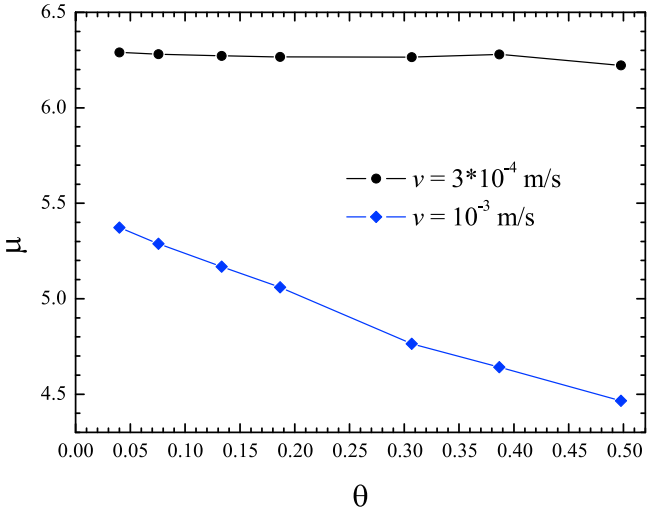

Fig. 7. Dependence of the friction coefficient μ on θ for two values of the driving velocity: $v = 3 \times 10^{-4}$ m/s (black circles) and $v = 10^{-3}$ m/s (blue diamonds). (For interpretation of the references to colour in this figure legend, the reader is referred to the Web version of this article.)

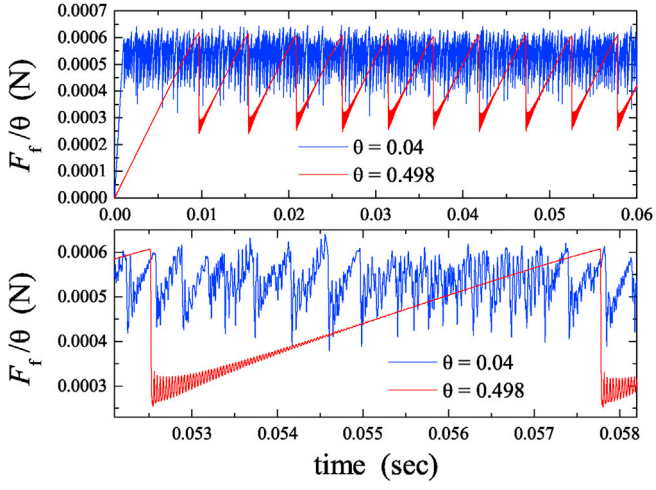

Fig. 8. Friction force F_f/θ versus time for two values of θ, $\theta = 0.04$ (blue) and $\theta = 0.498$ (red curve), for the driving velocity $v = 10^{-3}$ m/s. (For interpretation of the references to colour in this figure legend, the reader is referred to the Web version of this article.)

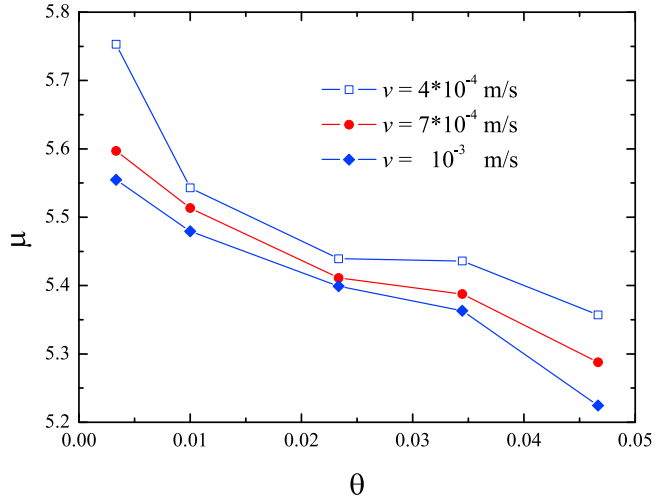

Fig. 9. Dependence of the friction coefficient μ on θ for three values of the driving velocity: $v = 4 \times 10^{-4}$ m/s (open squares), $v = 7 \times 10^{-4}$ m/s (red circles) and $v = 10^{-3}$ m/s (blue diamonds). (For interpretation of the references to colour in this figure legend, the reader is referred to the Web version of this article.)

smaller than $\langle f(v, v_i^*) \rangle$, because some contacts with $v_i^* < v$ undergo stick-slip. This situation corresponds to the $\theta \to 0$ limit (low load), when the contacts are far away from each other. However, at large θ (load) some contacts occur close to one another, and if one of them undergoes stick-slip, it may stimulate the neighboring contacts to stick-slip as well—the number of stick-slip contacts increases with θ, and the total friction force decreases.

Fig. 8 shows the friction force normalized by the concentration of frictional contact region, F_f/θ, as a function of time for two values of θ, $\theta = 0.04$ (blue) and $\theta = 0.498$ (red curve). The results are for $v = 10^{-3}$ m/s. Note that for the large coverage case global stick-slip occurs. In the experiments we do not observe so large fluctuations (and no periodic stick-slip oscillations) in the friction force as observed in Fig. 8 for large load. We believe this is due to the small system size we use, and in particular to the fact that in our model the macroasperity size is the same

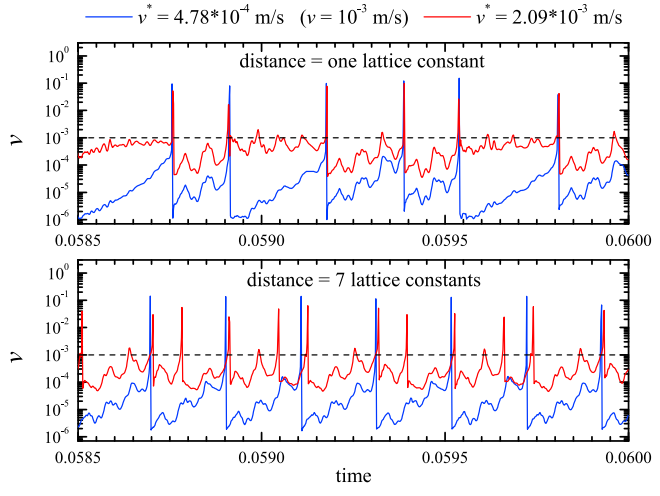

Fig. 10. The sliding speed as a function of time with the driving velocity $v = 10^{-3}$ m/s, for the case of only two frictional contact areas with the maximum in the friction at $v_1^* = 4.75 \times 10^{-4}$ m/s (blue curve) and $v_2^* = 2.09 \times 10^{-3}$ m/s (red curve). In (a) the frictional contacts occur on two nearby mass points (separated by one lattice constant), while in (b) they are separated by seven lattice constants. (For interpretation of the references to colour in this figure legend, the reader is referred to the Web version of this article.)

as the discretization length a. In order to get the elastic continuum limit correctly described, one should instead keep the size of the macroasperity contact regions fixed (say linear size R), and choose a discretization length a much smaller than R (i.e., $a/R \to 0$). Thus in a more accurate treatment we expect negligible global (on the block-level) stick-slip, at least as long as the macroasperity contact area is not close to the nominal contact area (i.e., $\theta = 1$). In other words, because of our small system size and the assumption $a = R$, the slip at different locations on the surface are strongly coupled, but for a larger system and with $R \gg a$ the different regions at large separation are weakly coupled and can slip more uncorrelated, which will reduce (due to self-averaging) the stick-slip on the block-size scale to a negligible value. In Fig. 7 we present the time-averaged friction force acting on the sliding block.

For the small system we study, as long as the drive velocity v is large enough that some frictional contact regions has a velocity maximum below v, we expect the macroscopic stick-slip to be non-negligible. This is consistent with the rather abrupt change we observe as v increases from below $10^{-3.5}$ m/s $\approx 3.16 \times 10^{-4}$ m/s (where steady sliding is observed) to above this value. This is illustrated in Fig. 9 which shows that even for $v = 4 \times 10^{-4}$ m/s the friction force is strongly reduced compared to the $v = 3 \times 10^{-4}$ m/s case in Fig. 7.

The strong coupling between the frictional contact regions within our sliding unit (with $N_x = N_y = 15$) is also illustrated in Fig. 10. We show the sliding speed as a function of time with the drive velocity $v = 10^{-3}$ m/s, for the case of only two frictional contact areas, with the maximum in the friction at $v_1^* = 4.75 \times 10^{-4}$ m/s (blue curve) and $v_2^* = 2.09 \times 10^{-3}$ m/s (red curve). In the top-figure (case (a)) the frictional contacts occur on two nearby mass points (separated by one lattice constant), while in the bottom figure (case (b)) they are separated by seven lattice constants. Note that because of the elastic coupling between the contact regions, the contact region with $v_2^* = 2.09 \times 10^{-3}$ m/s (red curve) performs stick-slip like motion in spite of the fact that it would move with a constant velocity if it would be the only contact region at the interface. In case (a), where the contact regions occur on nearby mass points, the motion of the two contact areas are fully synchronized (both contact regions undergo large velocity slip at the same time), while in case (b) the contact region with $v_2^* = 2.09 \times 10^{-3}$ m/s (red curve) undergoes stick-slip at a higher frequency, and never at exactly the same time as for the $v_1^* = 4.75 \times 10^{-4}$ m/s contact region (blue curve) (the peaks in the velocity, for those slip events where the two contact regions slip at nearly the same time, are separated by roughly the time it takes for an elastic wave to propagate a distance corresponding to 7 lattice constants).

6. Summary and conclusion

The experimental results in Refs. [23] and [22] and also above show that the rubber friction coefficient $\mu(v)$, in a narrow velocity region around the velocity where $\mu(v)$ is maximal, depends on the nominal contact pressure p_0, even when the sliding speed is so low that frictional heating is unimportant. We attribute this effect to the coupling between the macroasperity contact regions. We have presented a model which shows that the lateral coupling between the macroasperity contact regions can enhance stick-slip of the contact regions. Since the average distance between two nearby macroasperity contact region decreases when the load increases, the lateral coupling increases, and the friction coefficient decreases, as the load increases.

The mechanism for the dependency of the friction coefficient on the load considered here is very general, and is also relevant for non-rubber materials, i.e., for any multi-contact interface. The stick-slip of the macroasperity contact regions should manifest itself in the power spectrum of the block velocity, and in the acoustic power spectrum, so studying these quantities should be one way to test the hypothesis presented above. Simulations for larger systems and different sets of parameters are also desirable, and we plan to proceed in this way in future.

Acknowledgments

The research work was performed within a Reinhart-Koselleck project funded by the Deutsche Forschungsgemeinschaft (DFG). We would like to thank DFG for the project support under the reference German Research Foundation DFG-Grant: MU 1225/36-1. The research work was also supported by the DFG-grant: PE 807/10-1. This work is supported in part by COST Action MP1303.

References

[1] Rabinowicz E. Friction and wear of materials. second ed. New York: Wiley; 1995.
[2] Persson BNJ. Sliding friction: physical principles and applications. second ed. Heidelberg: Springer; 2000.
[3] Gnecco E, Meyer E. Elements of friction theory and nanotribology. Cambridge: Cambridge University Press; 2015.
[4] Persson BNJ. Theory of rubber friction and contact mechanics. J Chem Phys 2001; 115:3840.
[5] Persson BNJ. Contact mechanics for randomly rough surfaces. Surf Sci Rep 2006;61: 201.
[6] Hyun S, Pei L, Molinari JF, Robbins MO. Finite-element analysis of contact between elastic self-affine surfaces. Phys Rev E 2004;70, 026117.
[7] Campana C, Müser MH. Contact mechanics of real vs. randomly rough surfaces: a Green's function molecular dynamics study. Europhys Lett 2007;77:38005.
[8] Yastrebova VA, Anciaux G, Molinari JF. From infinitesimal to full contact between rough surfaces: evolution of the contact area. Int J Solid Struct 2015;52:83.
[9] Persson BNJ, Sivebaek IM, Samoilov VN, Zhao K, Volokitin AI, Zhang Z. On the origin of Amonton's friction law. J Phys Condens Matter 2008;20:395006.
[10] Almqvist A, Campana C, Prodanov N, Persson BNJ. Interfacial separation between elastic solids with randomly rough surfaces: comparison between theory and numerical techniques. J Mech Phys Solid 2011;59:2355.
[11] Pastewka L, Robbins MO. Contact between rough surfaces and a criterion for macroscopic adhesion. Proc Natl Acad Sci Unit States Am 2014;111:3298.
[12] Persson BNJ, Scaraggi M. Theory of adhesion: role of surface roughness. J Chem Phys 2014;141, 124701.
[13] Persson BNJ. Rubber friction and tire dynamics. J Phys Condens Matter 2011;23, 015003.
[14] Selig M, Lorenz B, Henrichmöller D, Schmidt K, Ball A, Persson BNJ. Rubber friction and tire dynamics: a comparison of theory with experimental data. Tire Sci Technol 2015;42:216.
[15] Burridge R, Knopoff L. Model and theoretical seismicity. Bull Seismol Soc Am 1967; 57:341.
[16] Persson BNJ. Theory of friction: stress domains, relaxation, and creep. Phys Rev B 1995;51, 13568.
[17] Braun OM. Bridging the gap between the atomic-scale and macroscopic modeling of friction. Tribol Lett 2010;39:283.
[18] Braun OM, Tosatti E. Kinetics of stick-slip friction in boundary lubrication. Europhys Lett 2009;88, 48003.
[19] Braun OM, Tosatti E. Kinetics and dynamics of frictional stick-slip in mesoscopic boundary lubrication. Phil Mag 2011;91:3253.
[20] Braun OM, Peyrard M, Stryzheus DV, Tosatti E. Collective effects at frictional interfaces. Tribol Lett 2012;48:11.
[21] Persson BNJ. On the fractal dimension of rough surfaces. Tribol Lett 2014;54:99.
[22] Braun OM, Steenwyk B, Warhadpande A, Persson BNJ. On the dependency of friction on load: theory and experiment. Europhys Lett 2016;113, 56002.
[23] Fortunato G, Ciaravola V, Furno A, Scaraggi M, Lorenz B, Persson BNJ. On the dependency of rubber friction on the normal force or load: theory and experiment. Tire Sci Technol 2017;45:25. see also ArXiv:1512.01359.
[24] Lorenz B, Oh YR, Nam SK, Jeon SH, Persson BNJ. Rubber friction on road surfaces: experiment and theory for low sliding speeds. J Chem Phys 2015;142, 194701.
[25] Landau LD, Lifshitz EM. Theory of elasticity. New York: Pergamon; 1986.
[26] Braun OM, Tosatti E. Aftershocks in a frictional earthquake model. Phys Rev E 2014;90, 032403.